Inventory of Supplemental Information

Supplemental Figures

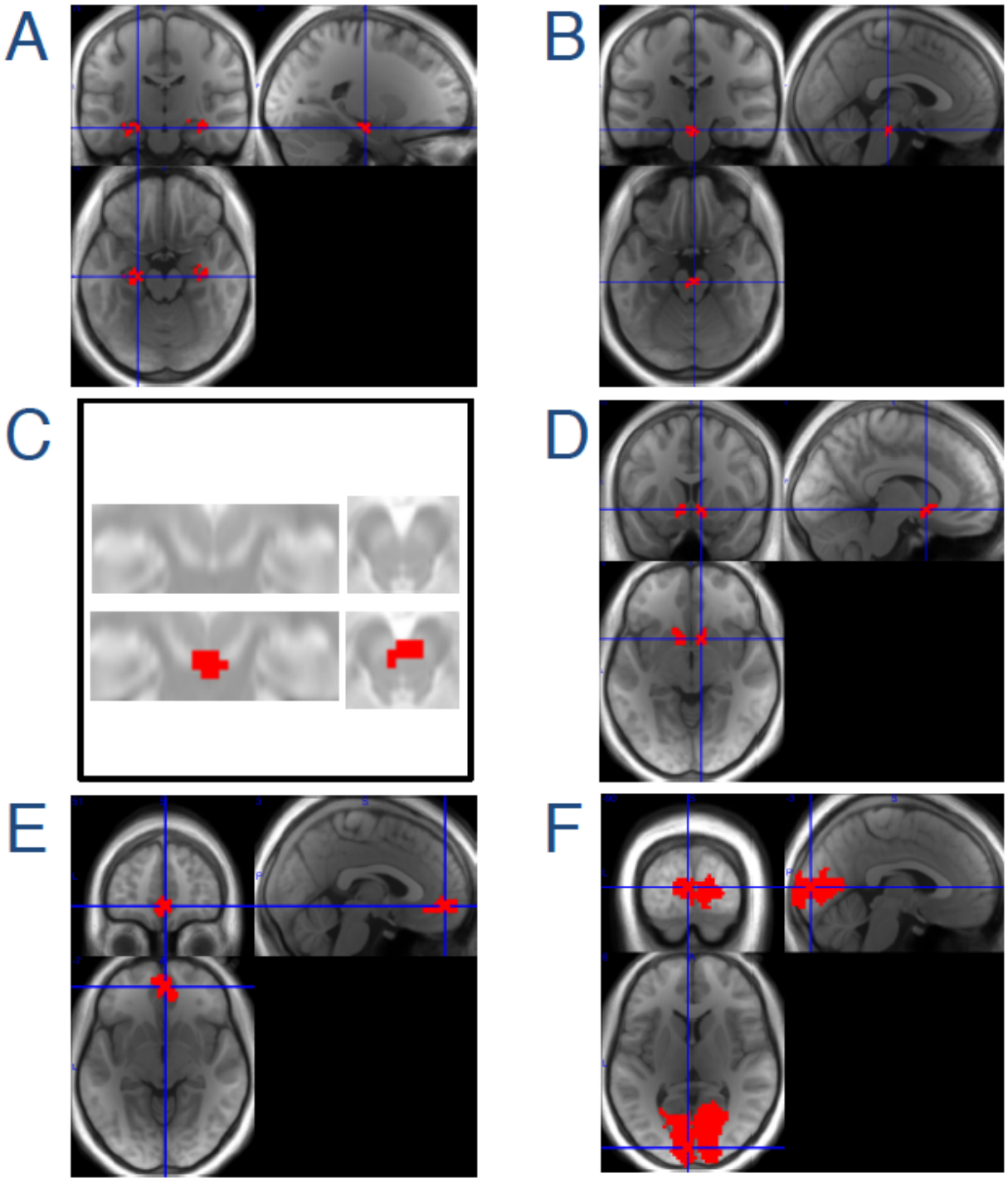

Figure S1. Overview of regions of interest (ROIs). For the bilateral ROI analyses, voxels were selected that functionally overlapped with anatomical masks: **(A)** the bilateral hippocampus (MNI: *x*=-21, *y*=-18, *z*=-19), **(B)** the bilateral SN/VTA (MNI: *x*=3, *y*=-23, *z*=-20), **(D)** the bilateral nucleus accumbens (MNI: *x*=9, *y*=10, *z*=-6), **(E)** the bilateral ventromedial prefrontal cortex (MNI: *x*=3, *y*=51, *z*=-

7), and **(F)** for bilateral V1 (MNI: *x*=-3, *y*=-90, *z*=6). ROI clusters are shown for coronal, sagittal, and transverse slices on the average, normalized anatomical image in our group of participants. **(C)** The SN/VTA ROI is also shown on a magnetization transfer image (Bunzeck and Düzel, 2006). On these images, the SN/VTA complex is visible as a white band. Depicted are a coronal and a transverse slice (top) and the same slices overlaid with the SN/VTA ROI (bottom) for the same MNI coordinates as in (B).

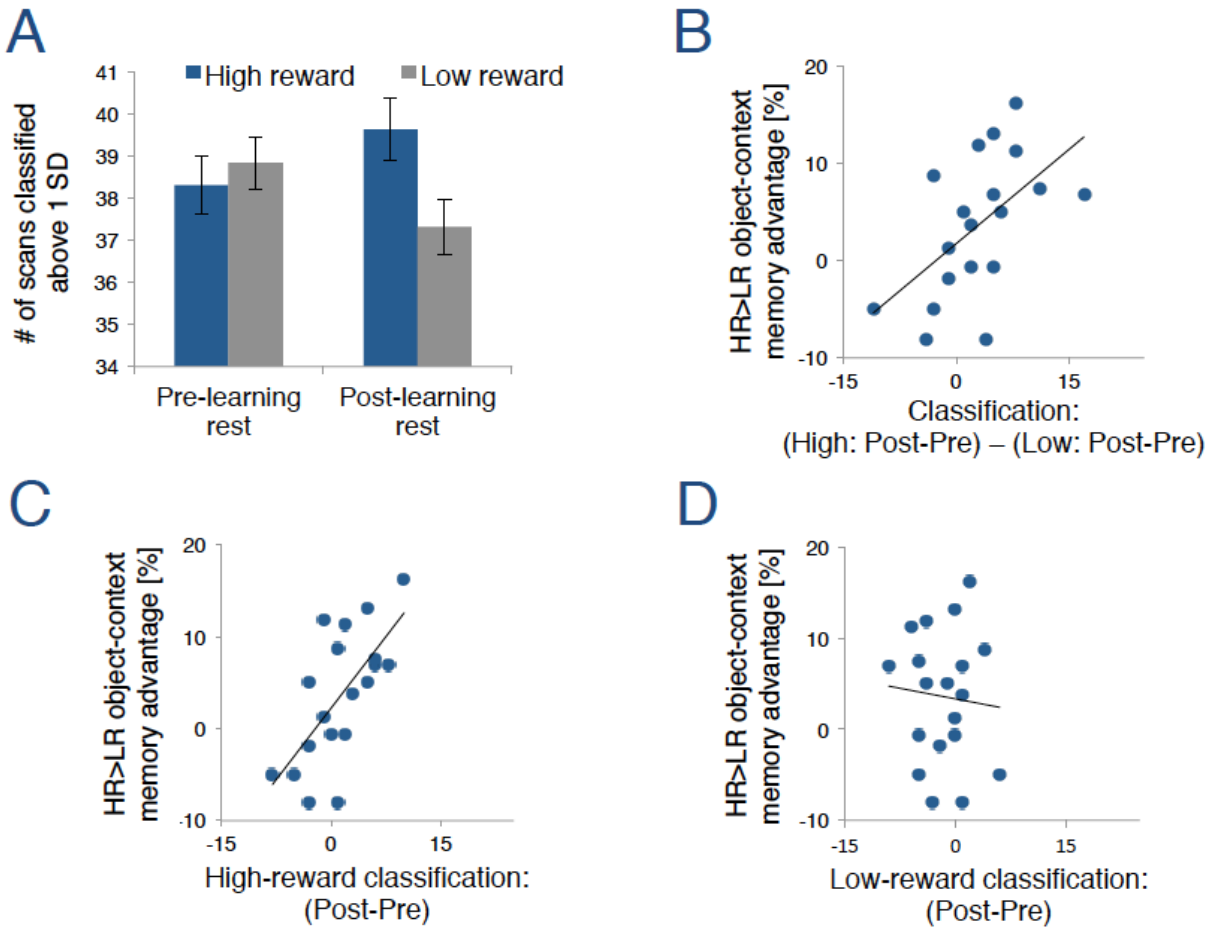

Figure S2 (related to Figure 3). Thresholded hippocampal reactivation analyses are in line with reactivation findings reported in the main text. (A) Instead of counting the number of all time points that were classified for high-reward context as in the main analyses reported in main text, we used a threshold (i.e. counting only events above 1SD within each condition) to separately identify hippocampal reactivation events associated with high- and low-reward contexts. Hippocampal reactivation events revealed significantly increased reactivation of high- compared to low-reward contexts during the post-learning rest, but not during the pre-learning rest period. **(B)** Using this threshold, a 'preferential high-reward reactivation index' (i.e. [(High reward: Post – Pre) – (Low reward: Post – Pre)]) positively correlated with the HR>LR object-context memory advantage. Follow-up analyses for high- and low-reward reactivation separately showed that only the increase in classifier predictions of high-reward contexts from pre- to post-learning rest was significantly correlated the HR>LR object-context memory advantage **(C)**, but the pre- to post-learning change in reactivation for low-reward contexts was not significantly correlated with the HR>LR object-context memory advantage **(D)**.

Table S1. Whole-brain analyses during reward-motivated learning task. For whole-brain, voxel-based analyses, we used 3DClustSim (Cox, 1996) to determine a cluster correction of $p<0.05$ for the whole brain ($p<0.001$ and $k=45$ voxels using a whole-brain mask based on the subjects' mean anatomical image). MNI coordinates for the peak voxels of significant clusters ($p<0.05$), along with their *t* values and voxel cluster size (3mm isotropic) (SMEs = subsequent memory effects; L = left hemisphere; R = right hemisphere).

Region	Cluster size	t(18)	MNI coordinates
Object-context memory SMEs (independent of reward)			
L inferior frontal gyrus and insula	1116	7.72	-39 24 -18
L inferior temporal gyrus	276	7.39	-51 -48 -15
L superior medial gyrus	134	6.69	-3 27 48
R inferior frontal gyrus	322	6.28	51 36 18
R inferior frontal gyrus and insula	118	5.66	30 36 -18
R supramarginal and postcentral gyrus	88	5.25	60 -24 48
R inferior temporal gyrus	134	5.17	48 -57 -15
Recollection SMEs (independent of reward)			
L inferior frontal gyrus	696	7.87	-33 30 -18
L hippocampus (cluster encompassing surrounding MTL cortex and amygdala)	233	7.61	-30 -15 -18
L inferior temporal and inferior occipital gyrus	289	7.16	-54 -45 -12
R inferior frontal gyrus	304	6.45	48 36 15
L superior medial gyrus	95	6.25	-9 39 42
R inferior temporal gyrus	119	5.19	57 -60 -3
R postcentral gyrus	46	4.37	57 -3 33

The interactions SME x Reward did not reveal any significant clusters surviving our cluster threshold.

Cue-related activation (High > Low reward)			
L/R middle cingulate cortex	345	7.54	3 15 36
L/R striatum	854	6.69	-12 15 -12
R hippocampus (cluster encompassing surrounding MTL cortex)	343	6.68	39 -12 -24
R insula	194	5.88	33 12 6
R precentral gyrus	112	5.78	39 -9 45
L thalamus	60	5.73	-24 -12 15
L/R precuneus	300	5.56	3 -54 48
R precentral gyrus	80	5.46	-45 -9 45
R middle occipital gyrus	55	5.30	30 -75 21
L cerebellum/ fusiform gyrus	153	5.20	-36 -57 -24
L superior occipital gyrus	82	5.08	-21 -63 27
L superior temporal gyrus	45	4.77	-63 -27 15

A Low > High reward contrast did not reveal any significant clusters surviving our cluster threshold.

Table S2. MVPA analyses: Encoding classification and reactivation analyses based on voxel patterns in further ROIs and across the whole brain. At the top panel, we show encoding classification results based on a 4-way classifier to distinguish between the four specific scene contexts (chance level = 25%). In the middle panel, we show encoding classification results based on a 2-way classifier to distinguish between high- and low-reward contexts (chance level = 50%). At the bottom panel, we show reactivation analyses based on a 2-way classifier to distinguish between reward contexts during pre- and post-learning rest periods. Means (SE) of encoding classification or reactivation 'classification' are shown along with their *t* and one-tailed *p* values of one-sample t-tests testing for significant differences from chance performance (chance level = 244 timepoints). NAcc, nucleus accumbens; vmPFC, ventromedial prefrontal cortex.

Region	**Classification**	***t*(18)**	***p***
Encoding-task classification (chance level = 25%)			
NAcc	26.0% (±0.2)	4.14	<0.001
vmPFC	26.3% (±0.5)	2.36	0.015
V1	42.5% (±1.1)	16.28	<0.001
1000 most discriminative whole-brain voxels	48.5% (±1.5)	15.15	<0.001
Reward-context classification (chance = 50%)			
NAcc	51.3% (±0.4)	3.22	0.004
vmPFC	52.2% (±0.7)	2.72	0.007
V1	73.8% (±1.1)	19.54	<0.001
1000 most discriminative whole-brain voxels	78.7% (±1.5)	18.83	<0.001

High-reward ‘classification’ (chance level = 244 timepoints)			
NAcc			
Pre-learning rest	245.3 (±1.6)	0.81	0.215
Post-learning rest	242.3 (±1.5)	-1.13	0.137
vmPFC			
Pre-learning rest	244.5 (±1.7)	0.31	0.379
Post-learning rest	244.7 (±1.8)	0.41	0.342
V1			
Pre-learning rest	246.1 (±1.9)	1.11	0.141
Post-learning rest	244.9 (±1.3)	0.69	0.249
1000 most discriminative whole-brain voxels			
Pre-learning rest	246.8 (±1.8)	1.51	0.074
Post-learning rest	242.6 (±1.3)	-1.06	0.152

Table S3. Resting-state functional connectivity: whole-brain analyses and further ROI analyses. At the top, whole-brain RSFC analyses with the hippocampal ROI as seed region. Using the same whole-brain cluster correction as for the analyses shown in Table S1, we did not find any significant clusters. An exploratory analysis shows MNI coordinates for the peak voxels of significant clusters surviving a liberal statistical threshold (p<0.005 uncorrected, k=10 voxels), along with their t values and voxel cluster size (3mm isotropic) (L = left hemisphere; R = right hemisphere). In the middle and at the bottom panel, ROI RSFC analyses with the hippocampal ROI as seed (middle panel) and the SN/VTA ROI as seed (bottom panel). Averaged *Pearson's r* (SE) indexing RSFC are shown for pre- and post-learning rest periods along with their t and one-tailed p values of paired-sample t-tests testing for significant RSFC changes. In addition, *Pearson's r* along with one-tailed p values are shown testing the correlations between RSFC change and the HR>LR object-context memory advantage.

Region	Cluster size	t(18)	MNI coordinates
Whole-brain RSFC changes with hippocampal ROI as seed region (post-learning > pre-learning rest period)			
L/R anterior cingulate cortex	74	4.20	-3 30 24
R insula	22	3.86	33 9 -6
L insula	30	3.69	-36 12 -6
thalamus	10	3.67	-9 -12 0
R inferior frontal gyrus	26	3.05	48 24 0

RSFC between hippocampal ROI and further ROIs				
ROIs	**Pre-learning**	**Post-learning**		
NAcc-hippocampus	*r*=0.177 (±0.037)	*r*=0.232 (±0.042)	*t*(18)=1.23	*p*=0.117
Correlation between RSFC change and HR>LR object-context memory advantage:			*r*=0.146	*p*=0.275
vmPFC-hippocampus	*r*=0.390 (±0.031)	*r*=0.365 (±0.062)	*t*(18)=-0.16	*p*=0.437
Correlation between RSFC change and HR>LR object-context memory advantage:			*r*=-0.008	*p*=0.487
V1-hippocampus	*r*=-0.077 (±0.043)	*r*=-0.065 (±0.055)	*t*(18)=0.20	*p*=0.423
Correlation between RSFC change and HR>LR object-context memory advantage:			*r*=-0.123	*p*=0.308

RSFC between SN/VTA ROI and further ROIs				
ROIs	**Pre-learning**	**Post-learning**		
NAcc-SN/VTA	*r*=0.229 (±0.037)	*r*=0.237 (±0.039)	*t*(18)=0.20	*p*=0.424
Correlation between RSFC change and HR>LR object-context memory advantage:			*r*=0.287	*p*=0.117
vmPFC- SN/VTA	*r*=0.234 (±0.043)	*r*=0.196 (±0.043)	*t*(18)=-0.94	*p*=0.179
Correlation between RSFC change and HR>LR object-context memory advantage:			*r*=-0.076	*p*=0.379
V1- SN/VTA	*r*=-0.004 (±0.025)	*r*=0.031 (±0.046)	*t*(18)=0.78	*p*=0.224
Correlation between RSFC change and HR>LR object-context memory advantage:			*r*=-0.056	*p*=0.410

Supplemental fMRI analyses

Reward context enhances cue-related activation in the SN/VTA and hippocampus during learning

To better characterize whether encoding-related activity in our paradigm is consistent with previous findings on reward anticipation, we analyzed activity elicited by reward cues, and tested whether activation in the bilateral SN/VTA and hippocampus ROIs was increased in high compared to low reward contexts. Paralleling findings of previous studies on reward anticipation (Adcock et al., 2006; Knutson et al., 2001; Murty and Adcock, 2014), we found that activity in both the bilateral SN/VTA ($t_{(18)}$=2.69, p=0.007) and bilateral hippocampus ROIs ($t_{(18)}$=3.03, p=0.004) was increased during processing of high reward cues relative to low reward cues. Additional whole-brain, voxel based analyses revealed a widespread network of enhanced activation for high- compared to low-reward cues (**Table S1**).

Thresholded analyses on hippocampal reactivations are in line with reactivation findings reported in the main text

One limitation of the analysis reported in the main text is that voxel patterns at every single time point were classified as corresponding to high- or low-reward contexts, regardless of the strength of evidence. Given that we would not expect reactivation events to occur at every time point, we therefore ran a further complementary analysis in which we used a more stringent threshold for identifying reactivation of a study context, based on the strength of the prediction from the pattern classifier. Specifically, we defined "reactivation events" as only occurring at time points in which the classifier evidence was more than one standard deviation (SD) above the condition-specific mean classifier evidence (i.e. 1 SD above the low-reward mean and 1 SD above the high-reward mean). The 1 SD threshold was chosen because it allowed us to identify enough reactivation events to analyze reactivation for high- and low-reward contexts and to investigate whether there was increased reactivation of high-

compared low-reward contexts during post-learning rest (using a one-tailed paired-sample *t*-test). In line with our previous analyses, we found that, during post-learning rest, the frequency of reactivation events was significantly higher for high-reward than for low-reward contexts (39.6 SE=±0.75 vs. 37.3 SE=±0.65, respectively; $t_{(18)}$=1.99, p=0.031; **Figure S2A**). In contrast, we did not observe a significant between-condition difference in the frequency of "reactivation events" during pre-learning rest (38.3 SE=±0.70 vs. 38.8 SE=±0.62, respectively; $t_{(18)}$=-0.54, p>0.05; **Figure S2A**), which rules out the possibility that the post-learning effect was driven by biases in the classifier. We next investigated the relationship between preferential reactivation of high-reward contexts and the HR>LR object-context memory advantage. Similar to the analyses in the main text, we first computed a "preferential reactivation index". Here, this preferential reactivation index relates differences between reactivation of high- and low-reward contexts to individual differences, while controlling for overall classifier prediction biases. Specifically, we computed the change in reactivation from pre- to post-learning rest separately for high- and low-reward contexts, and then computed the difference between the number of reactivations for high- and low-reward contexts (i.e. (High reward: Post- – Pre-learning rest) – (Low reward: Post- – Pre-learning rest). In line with the findings reported in the main text, we observed a significant positive correlation between the preferential reactivation index and the HR>LR object-context memory advantage (*Pearson's* r=0.553, p=0.007; **Figure S2B**). Follow-up analyses suggested that this positive relationship between hippocampal reactivations and object-context memory advantage was driven by reactivation of high-reward contexts. That is, the increase in classifier predictions of high-reward contexts from pre- to post-learning rest was significantly correlated with the HR>LR object-context memory advantage (*Pearson's* r=0.669; p=0.001; **Figure S2C**). In contrast, the pre- to post-learning change in hippocampal reactivation of low reward contexts was not significantly correlated with HR>LR object-context memory advantage (*Pearson's* r=-0.080; p>0.05; **Figure S2D**). The latter two correlation coefficients significantly differed (z=2.46,

p=0.014) suggesting a selective relationship between high-reward reactivation and the later HR>LR object-context memory advantage.

Hippocampal encoding activity and changes in SN/VTA-hippocampal RSFC uniquely contribute to HR>LR recollection advantage

In the main text, we showed that the HR>LR *object-context memory* advantage was associated with increases in SN/VTA-hippocampal RSFC and hippocampal reactivations, and could not be explained by hippocampal encoding-related activity. Because we also found a HR>LR *recollection* advantage, we ran a complementary hierarchical regression analysis testing how individual differences in learning and post-learning effects contributed to the HR>LR *recollection* advantage (using the same analysis approach as reported in the main text testing for HR>LR object-context memory advantage). In the first step, we tested the extent to which these individual differences could be accounted for by hippocampal encoding-related activity alone (i.e. the Reward x SME interaction; SME: Recollected vs. Forgotten). This *encoding-only model* explained 28.6% of the variance in HR>LR recollection advantages ($F_{(1,17)}$=6.82; *p*=0.018), indicating that hippocampal encoding-related activity was significantly related to the HR>LR *recollection* advantage. In the next step, we added individual pre-to-post learning changes in SN/VTA-hippocampal RSFC to the model. This *encoding + RSFC model* explained 80.5% of the variance in contributing to the HR>LR recollection advantage, which is significantly higher than what was explained by the *encoding-only* model ($F_{(1,16)}$=42.53; *p*<0.001). Finally, we added individual differences in the high-reward reactivation index to the model. This *encoding + RSFC + reactivations model* explained 81.1% of the variance, which is not significantly higher than what was explained by the *encoding + RSFC* model ($F_{(1,15)}$=0.46; *p*=0.508). Examination of the three-predictor model showed that hippocampal encoding (related to later recollection) and SN/VTA-hippocampal RSFC changes significantly predicted the HR>LR recollection advantage ($t_{(15)}$=5.21 and $t_{(15)}$=6.42, respectively; *p's*<0.001), but hippocampal reactivations did not significantly contribute to the overall model

($t_{(15)}$=0.68, p=0.254). Consistent with the findings explaining the HR>LR object-context memory advantage (reported in the main text), the findings demonstrate that the relationship between later HR>LR recollection advantage and post-learning dynamics (here, specific to SN/VTA-hippocampal RSFC changes) could not be explained by hippocampal encoding-related activity.

In addition, adding overall recollection (independent of reward) as a fourth predictor to the three-predictor model did not significantly change the overall model fit compared to the three-predictor model ($F_{(1,14)}$=0.27; p=0.613). Most importantly, in this four-predictor model (*encoding + RSFC + reactivations + overall memory model*), both the hippocampal encoding activity and the SN/VTA-hippocampal RSFC changes still remained significant predictors of the HR>LR recollection advantage ($t_{(14)}$=4.68 and $t_{(14)}$=5.80, respectively; *p's*≤0.001).

Supplemental Experimental Procedures

Participants

Twenty healthy young adults took part in the experiment. One participant was excluded from the analyses due to excessive movement artifacts in the fMRI data. Results are based on the remaining nineteen participants (10 female and 9 male participants). Participants' mean age was 23.7 years (range: 18-32). Eighteen participants were right-handed and one participant was left-handed. Importantly, inclusion or exclusion of the data from the left-handed participant did not alter any main interpretations of our findings. They were compensated with $40 for their total time in the laboratory and an additional reward based on performance during the encoding phase (average: $23.60; range: $20.40-$25.45). All participants had normal or corrected-to-normal vision and were native English speakers. The UC Davis Institutional Review Board approved the experiment.

Material

Object stimuli were obtained from a publicly available database (http://cvcl.mit.edu/MM/uniqueObjects.html) (Brady et al., 2008). The 320 objects were used for the encoding phase. They were split into four sets of 80 objects each for the four encoding judgments. The four item sets were counterbalanced across the high and low reward conditions with the restriction that the "basketball" and "floating" judgments were always used together for either high or low reward. The "laptop" and "juggling" judgment were always paired together for the other reward condition. In half of the participants, two item sets (A and B) were used for the "basketball" and "floating" judgments and the other two item sets (C and D) were used for the "laptop" and "juggling" judgments. This was vice versa in the other half of participants: that is, items sets C and D for "basketball" and "floating" judgments and item sets A and B for judgments "laptop" and "juggling". Independent of the counterbalancing, yes/no

responses were roughly equalized in each set. If it was ambiguous about whether a 'yes' or 'no' response would be correct, both responses were rewarded (unknown to the participant). An additional item set containing 120 objects was used as distractors during the test phase.

Behavioral analyses

For behavioral performance during the learning phase, we used two-tailed paired-sample *t*-tests to statistically compare accuracy and reaction times for semantic judgments between high and low reward conditions. To statistically assess whether memory for objects *improved* for the high compared to the low reward condition, we performed one-tailed paired-sample *t*-tests. Based on dual-process models of recognition memory (Yonelinas, 2002), we estimated recognition based on recollection and familiarity. For recollection, we computed Hits – False Alarms for the 'remember' responses. For familiarity, we used 'confident old and 'unconfident old' (i.e. 5 and 4) responses and corrected for recollection by computing: [(54(old item)/1-R(old item)) - (54(new item)/1-R(new item))]. The findings did not change significantly if familiarity estimation was restricted to 'confident old' responses. For memory accuracy for object-context associations, we computed Hits (i.e. correct object-context association) – False Alarms (i.e. incorrect object-context association).

FMRI acquisition

We used a 3T Siemens Skyra scanner with a 32-channel phased array head coil to acquire anatomical and functional MRI images. A multiband Echo-Planar Imaging sequence was used to acquire whole brain T_2*-weighted images (TR=1.22 s, TE=24ms; 38 slices per volume; multiband factor=2; voxel size=3 mm isotropic). In addition, a T1-weighted MP-RAGE with whole brain coverage was acquired. Inside the head coil, the participant's head was padded to restrict excessive motion. Stimuli were displayed on a mirror attached to the head coil above the participant's eyes. During the scanning, the participant's eyes were monitored by the experimenter via an eye tracker that was set up to ensure that the participant attended

to all stimuli and to not close the eyes during the rest periods. The encoding phase contained 10 scanning runs with 215 scans each and the rest phases were acquired in one run each containing 492 scans.

FMRI preprocessing

The functional and anatomical images were preprocessed and analyzed using the SPM8 software (The Wellcome Trust Centre for Neuroimaging, London, UK). The functional images were first realigned and then coregistered to the anatomical images. Anatomical images were segmented into grey and white matter images and imported into DARTEL to create a template anatomical image that was specific to the participants in this study. We then used DARTEL to normalize functional and anatomical images into MNI space. For all ROI analyses using RSFC and MVPA, we used unsmoothed functional images. The ART repair toolbox (http://cibsr.stanford.edu/tools/human-brain-project/artrepair-software.html) was used to identify individual scans that showed abrupt motion or signal fluctuations. Details of specific preprocessing steps are described in the individual Methods section for RSFC and MVPA analyses (see Methods in main text). Note that we corrected for slow and abrupt head movements in all analyses, but we were not able to correct for artifacts driven by cardio-respiratory effects.

Regions-of-interest approach

Given the established roles of the hippocampus in binding item and context information (Diana et al. 2007; Eichenbaum et al. 2007), in coordinating memory reactivation (Sutherland & McNaughton 2000; Carr et al. 2011; Káli & Dayan 2004), and of the SN/VTA in signaling reward and salience (Haber & Knutson 2010; Shohamy & Adcock 2010), we reasoned that reward-motivated learning might lead to enhanced interactions between these regions during offline post-learning rest periods. Therefore, we focused our main analyses on two main regions of interest (ROIs): the hippocampus and the SN/VTA.

As in our previous work (Gruber et al. 2014), we used a hippocampal ROI including voxels that have been reliably implicated in reward processing. Using the NeuroSynth tool (neurosynth.org) (Yarkoni et al. 2011), we performed a term-based search on "reward" that included 329 studies (retrieved: July 2nd 2013) and generated a reverse inference mask (i.e. probability of the term "reward" given the observed activation). We then inclusively masked this functional "reward" mask and an anatomical hippocampus mask from the SPM Anatomy Toolbox (Amunts et al. 2005). **Figure S1A** shows the resulting bilateral hippocampal ROI that indicate the overlap between the functional "reward" mask and the anatomical mask. Furthermore, the bilateral SN/VTA ROI was defined by identifying voxels that showed significant functional connectivity with the hippocampal ROI (i.e. seed region) during pre-learning rest. In order to have a sensitive measure, we selected clusters within the SN/VTA ROIs that survived whole-brain correction (FWE $p<0.05$). As for the hippocampus ROI, we then inclusively masked this functional mask within the SN/VTA with an anatomical ROI. For the bilateral SN/VTA ROI (**Figure S1B-C**), the anatomical mask was derived from a probabilistic mask based on magnetization transfer images (Guitart-Masip et al. 2011) containing the whole SN/VTA complex.

Because the nucleus accumbens (NAcc) and the ventromedial prefrontal cortex (vmPFC) are known to play an important role in reward processing and might also support reactivation and processes associated with consolidation (Frankland and Bontempi 2005; Kahn and Shohamy, 2013; Preston and Eichenbaum 2013), we additionally investigated how bilateral NAcc (**Figure S1D**) and vmPFC ROIs (**Figure S1E**) might support reactivation of reward contexts. For both NAcc and vmPFC ROIs, we used again the intersection between the functional "reward" mask (derived from neurosynth.org; as for the hippocampal ROI) and an anatomical mask (for further details regarding the NAcc ROI, cf. Gruber et al., 2014). For the vmPFC ROI, we ensured that the ROI did not extend posteriorly into the anterior cingulate cortex. In addition, we added a bilateral V1 ROI (**Figure S1F**) that was based on an anatomical, probabilistic mask from the SPM Anatomy Toolbox.

Whole-brain MVPA analyses

Additional analyses were performed to test how voxels across the whole brain would be sensitive to precise encoding contexts or general reward contexts. We therefore used a whole-brain approach that has been used previously to investigate post-learning reactivation (cf. Deuker et al., 2013). Instead of training a classifier on all voxels within a specific ROI, we ran an ANOVA as a feature selection step to determine the 1000 most predictive voxels across the brain dissociating between the precise encoding contexts (4-way classifier) and between the reward contexts (2-way classifier). All other MVPA analyses steps were identical to the analyses in the ROIs. Results of this whole-brain approach are summarized in **Table S3** and **S5**.

References

Adcock, R.A., Thangavel, A., Whitfield-Gabrieli, S., Knutson, B., and Gabrieli, J.D.E. (2006). Reward-motivated learning: mesolimbic activation precedes memory formation. Neuron *50*, 507–517.

Amunts, K., Kedo, O., Kindler, M., Pieperhoff, P., Mohlberg, H., Shah, N.J., Habel, U., Schneider, F., and Zilles, K. (2005). Cytoarchitectonic mapping of the human amygdala, hippocampal region and entorhinal cortex: intersubject variability and probability maps. Anat Embryol *210*, 343–352.

Brady, T.F., Konkle, T., Alvarez, G.A., and Oliva, A. (2008). Visual long-term memory has a massive storage capacity for object details. Proceedings of the National Academy of Sciences *105*, 14325–14329.

Bunzeck, N., and Düzel, E. (2006). Absolute coding of stimulus novelty in the human substantia nigra/VTA. Neuron *51*, 369–379.

Carr, M.F., Jadhav, S.P., and Frank, L.M. (2011). Hippocampal replay in the awake state: a potential substrate for memory consolidation and retrieval. Nat Neurosci *14*, 147–153.

Cox, R.W. (1996). AFNI: software for analysis and visualization of functional magnetic resonance neuroimages. Comput. Biomed. Res. *29*, 162–173.

Deuker, L., Olligs, J., Fell, J., Kranz, T.A., Mormann, F., Montag, C., Reuter, M., Elger, C.E., and Axmacher, N. (2013). Memory consolidation by replay of stimulus-specific neural activity. J. Neurosci. *33*, 19373–19383.

Diana, R.A., Yonelinas, A.P., and Ranganath, C. (2007). Imaging recollection and familiarity in the medial temporal lobe: a three-component model. Trends Cogn. Sci. (Regul. Ed.) *11*, 379–386.

Eichenbaum, H., Yonelinas, A.P., and Ranganath, C. (2007). The Medial Temporal Lobe and Recognition Memory. Annu. Rev. Neurosci. *30*, 123–152.

Frankland, P.W., and Bontempi, B. (2005). The organization of recent and remote memories. Nat Rev Neurosci *6*, 119–130.

Gruber, M.J., Gelman, B.D., and Ranganath, C. (2014). States of curiosity modulate hippocampus-dependent learning via the dopaminergic circuit. Neuron *84*, 486–496.

Guitart-Masip, M., Fuentemilla, L., Bach, D.R., Huys, Q.J.M., Dayan, P., Dolan, R.J., and Düzel, E. (2011). Action dominates valence in anticipatory representations in the human striatum and dopaminergic midbrain. J. Neurosci. *31*, 7867–7875.

Haber, S.N., and Knutson, B. (2010). The reward circuit: linking primate anatomy and human imaging. Neuropsychopharmacology *35*, 4–26.

Kahn, I., and Shohamy, D. (2013). Intrinsic connectivity between the hippocampus, nucleus accumbens, and ventral tegmental area in humans. Hippocampus *23*, 187-192.

Káli, S., and Dayan, P. (2004). Off-line replay maintains declarative memories in a model of hippocampal-neocortical interactions. Nat Neurosci *7*, 286–294.

Knutson, B., Adams, C.M., Fong, G.W., and Hommer, D. (2001). Anticipation of increasing

monetary reward selectively recruits nucleus accumbens. J. Neurosci. *21*, RC159.

Murty, V.P., and Adcock, R.A. (2014). Enriched encoding: reward motivation organizes cortical networks for hippocampal detection of unexpected events. Cereb. Cortex *24*, 2160–2168.

Preston, A.R., and Eichenbaum, H. (2013). Interplay of hippocampus and prefrontal cortex in memory. Curr. Biol. *23*, R764–R773.

Shohamy, D. (2011). ScienceDirect.com - Current Opinion in Neurobiology - Learning and motivation in the human striatum. Curr. Opin. Neurobiol.

Sutherland, G.R., and McNaughton, B. (2000). Memory trace reactivation in hippocampal and neocortical neuronal ensembles. Curr. Opin. Neurobiol. *10*, 180–186.

Yarkoni, T., Poldrack, R.A., Nichols, T.E., Van Essen, D.C., and Wager, T.D. (2011). Large-scale automated synthesis of human functional neuroimaging data. Nat. Methods *8*, 665–670.

Yonelinas, A.P. (2002). The Nature of Recollection and Familiarity: A Review of 30 Years of Research. Journal of Memory and Language *46*, 441–517.